# On Topology Optimization Strategies for Ultra-Compact High Contrast Grating Design

Jacob M. Hiesener, Robert P. Pesch, and Stephen E. Ralph, *Senior Member, IEEE*

***Abstract*— We describe a design methodology for optimizing an ultra-compact 3 $\mu$m long circular high contrast grating (HCG) reflector. A multi-stage optimization process involving parameter optimization (PO) followed by seeded topology optimization (TO) is demonstrated to design a device with performance better than that achieved with PO or TO alone. The device is designed for a foundry process and offers reflection commensurate with waveguide-based Bragg gratings with a significantly higher bandwidth in an ultra-compact footprint. A peak reflectance of 98.9 % was simulated centered at 1569 nm with a minimum reflectance of 97.9 % over C-band.**

***Index Terms*— Topology optimization (TO), silicon photonics, high contrast grating (HCG), inverse design.**

## I. Introduction

OPTICAL mirrors are a fundamental building block for all integrated photonics platforms. Bragg gratings are interferometric structures created with wavelength scale periodic variations in effective index typically achieved through a corrugated waveguide geometry [1]. Waveguide-based Bragg gratings are commonly used as optical mirrors for many applications including optical filtering, sensing, and integrated lasers [2], [3], [4], [5]. Many of these applications require a high reflectance in a compact footprint, which can be accomplished using a high contrast grating (HCG). HCGs operate similarly to waveguide-based Bragg gratings but use larger variations in effective index which increases the reflected power per unit length. Though HCGs are orders of magnitude smaller than waveguide-based Bragg gratings and ring loop mirrors, these devices can suffer more loss due to scattering and excitation of higher order modes. To mitigate loss due to scattering, circular HCG geometries have been designed and demonstrated to achieve high reflectance and bandwidth with a compact footprint [5]. However, the reflectance of these devices is often inferior to ring loop mirrors. In this work, we improve upon existing HCGs by decreasing the device footprint while further increasing the peak and average reflectance of the grating over C-band.

Topology optimization (TO) is a gradient-based inverse design methodology used to iteratively optimize every voxel of a device geometry to minimize a user-specified figure of merit (FOM). The resulting structure often exhibits physically nonintuitive features such as periodic ripples, low-index holes, and peripheral structures [6]. These features are often critical to the functionality of the device but may lead to design rule check (DRC) violations. As investigated in [6], a subset of the overall feature topology can be leveraged and re-optimized to yield higher performing, more compact structures.

We began by analytically designing a parameterized base model of the HCG for the GlobalFoundries (GF) Fotonix™ process informed by similar concave grating structures such as grating couplers. We performed initial simulations to validate the geometry and then performed parameter optimization (PO) to achieve a functional device geometry. Finally, the functional geometry was further optimized with a modified version of the TO methodology developed by Hammond et al. [7], yielding a dual optimized device with greater performance than is possible with conventional design methods.

## II. Physical Limits on Reflected Power

Any grating-based reflector has a limit on the reflected power based on the length and effective index contrast of the device. Coupled mode theory reveals that the peak reflectance for a Bragg grating (at the Bragg wavelength) is given by [8]:

$$R_{peak} = tanh^2(\kappa L) \tag{1}$$

$L$is the grating length and $\kappa$ is the coupling coefficient which, for an ideal rectangular grating profile, is [9]:

$$\kappa = 2\Delta n / \lambda_B \tag{2}$$

$\Delta n$ is the periodic effective index change given by $\Delta n = n_{eff2} - n_{eff1}$, where $n_{eff1,2}$ is the effective index of region 1 or 2 of the grating. $\lambda_B = 2\Lambda n_{eff}$ is the Bragg wavelength where $\Lambda$ is the grating period and $n_{eff} = (n_{eff1} + n_{eff2})/2$ is the average effective index of the grating. These results assume lossless, single mode operation with a fill factor of 0.5 (equal lengths of region 1 and region 2).

From these equations we can calculate the theoretical reflectance as a function of grating length and the effective

Manuscript received 10 January 2024; revised 20 February 2024; accepted 28 February 2024. Date of publication 1 March 2024; date of current version 4 April 2024. This work was supported in part by the National Science Foundation Center "Electronic and Photonic Integrated Circuits for Aerospace (EPICA)," (https://epica.research.gatech.edu) under Grant 2052808; and in part by Georgia Tech Partnership for an Advanced Computing Environment (PACE). *(Corresponding author: Stephen E. Ralph.)*

The authors are with Georgia Institute of Technology, Atlanta, GA 30332 USA (e-mail: jhiesener3@gatech.edu; rpesch6@gatech.edu; stephen.ralph@ece.gatech.edu).

Color versions of one or more figures in this letter are available at https://doi.org/10.1109/LPT.2024.3372429.

Digital Object Identifier 10.1109/LPT.2024.3372429

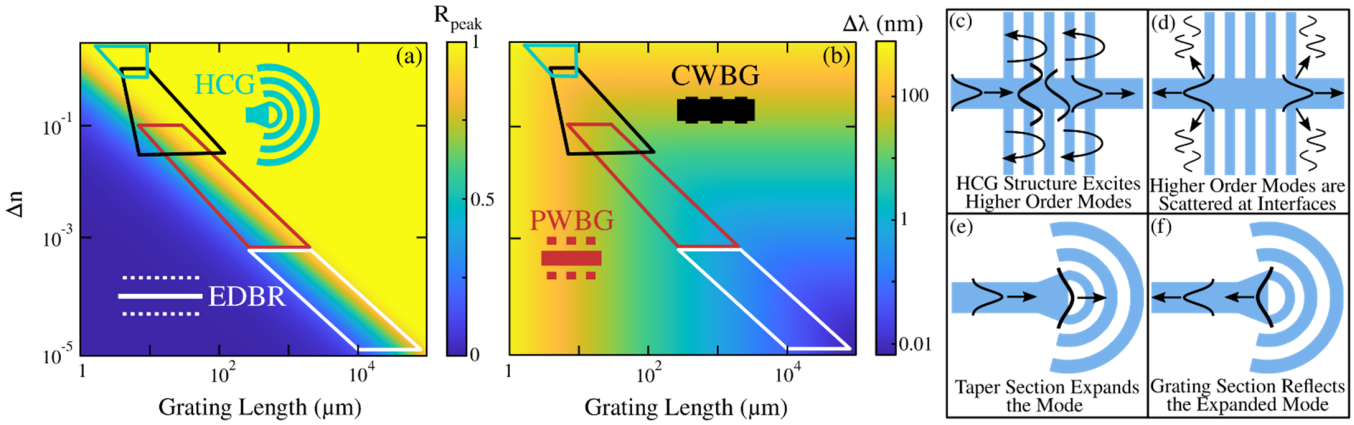


Fig. 1. Reflectance (a) and bandwidth (b) vs grating length and periodic effective index difference for a Bragg wavelength of 1550 nm and a group index of 4. Regions of operation for HCGs, corrugated waveguide Bragg gratings (CWBG), post waveguide Bragg gratings (PWBG), and extended distributed Bragg reflectors (EDBR) are marked. This is used as a guide for Bragg grating design. (c-d) Excitation of higher order mode in a HCG structure resulting in loss. (e-f) Operation of proposed circular HCG.

index (Fig. 1a). The bandwidth between nulls in the response of a Bragg grating is [8]:

$$\Delta\lambda = \frac{\lambda_B^2}{\pi n_g}\left[\kappa^2 + \left(\frac{\pi}{L}\right)^2\right]^{1/2} \cong \frac{\kappa\lambda_B^2}{\pi n_g} \tag{3}$$

$n_g$ is the average group index of the Bragg grating (∼4 for a buried silicon waveguide). Using (3) we can calculate the theoretical bandwidth versus grating length and effective index (Fig. 1b). The bandwidth of the HCG is dominated by the coupling coefficient ($\kappa \gg \pi/L$); therefore, the above approximation is appropriate. Under the approximation in (3), bandwidth is linearly proportional to the effective index difference, resulting in a high bandwidth for a HCG structure. The theoretical peak bandwidth and reflectance both break down for high contrast structures where mode confinement becomes an issue.

To achieve high reflectance in a short length, a grating structure requires large index contrast (Fig. 1a). Recent work has demonstrated compact (15 $\mu$m) Bragg reflectors with an array of nanoholes (100 nm diameter) in a silicon waveguide [10]. Although the structure achieves a significant index contrast without supporting higher order modes it is not fabricable on most commercial foundries due to the minimum enclosed area constraint. The structures reported here support higher order modes, however coupling to these modes is suppressed by design allowing an even higher index contrast. If we extend the grating sections of a corrugated waveguide Bragg grating to increase the index contrast, higher order modes are excited and scattered, causing significant loss (Fig. 1c-d).

Instead, we employ a circular Bragg grating geometry that consists of concave gratings and a taper that shapes the mode entering the grating structure (Fig. 1e-f). The input waveguide mode must expand to ensure the phase front matches the grating radius; otherwise, significant loss is ensured. The field in the grating structure expands into the gratings, no longer confined to a rectangular waveguide mode, and is subsequently reflected into the taper.

## III. Ultra-Compact Reflector Design Methodology

We utilize a dual optimization approach which enables insight into the physics of this device, enabling superior performance to PO or TO alone. We began by developing the geometry for a parameterized device and then performed PO on that geometry to yield a functional device. Our in-house TO pipeline was modified and seeded with the functional design from the PO and optimized, resulting in the final dual optimized structure.

### A. Parameter Optimization

The circular HCG was simulated using Lumerical's 3D finite-difference time-domain (FDTD) solver [11]. This device consists of apodised concave gratings with a taper to shape the waveguide mode entering the grating region. The taper length ($L_{taper}$), taper width ($w_{taper}$), grating extension angle ($\theta$), and the grating pitches ($\Lambda_1$, $\Lambda_2$, $\Lambda_3$) are the parameters that define the device geometry (Fig. 2a). An elliptical geometry was tested for the gratings but was found to provide a lesser reflectance compared to circular geometry.

Preliminary PO studies revealed that a short taper is sufficient and extension of the gratings beyond the 15° had little effect on performance, therefore the taper length was set to 0.5 $\mu$m and the extension angle was set to 15°. The taper width and the first 3 grating pitches were selected as free variables for PO (Fig. 2a). More than 3 pitch parameters were tested but after $\Lambda_2$ the grating pitches converged to the same value, therefore only 3 parameters were used for the grating. The MATLAB function bayesopt [12] is employed using default optimization parameters to implement a Bayesian optimization [13] that minimizes the following figure of merit (FOM):

$$FOM = 1 - \frac{P_r}{P_{in}} \tag{4}$$

$P_r$ is the reflected power and $P_{in}$ is the input power. The device was simulated exclusively at 1550 nm during the optimization, the high index contrast ensures good performance

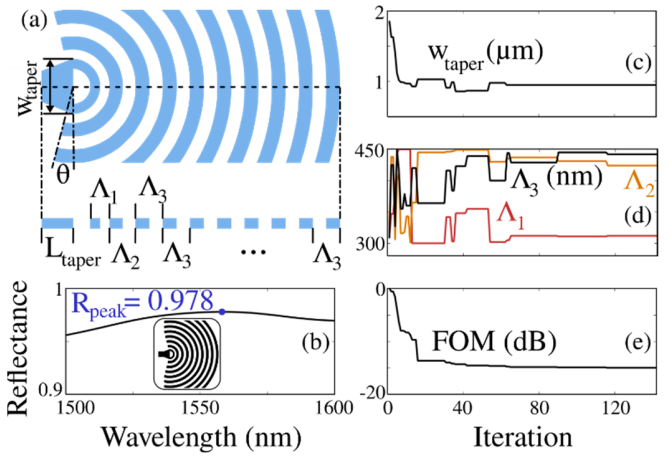


Fig. 2. (a) Diagram of the center section of the parameterized HCG with a cutaway of the center projected below. (b) Simulated reflectance spectrum of the parameterized HCG with the device shown in the inset. (c-e) Evolution of taper width, grating lengths, and the FOM during the optimization process.

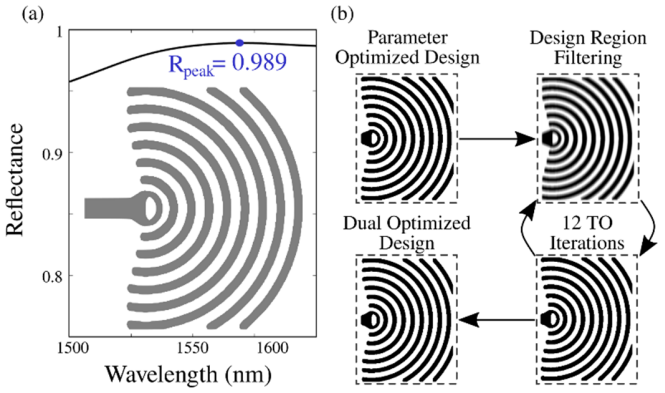


Fig. 3. (a) Simulated reflectance spectrum of topology optimized device; geometry shown in the inset. (b) Diagram of topology optimization pipeline.

over a large bandwidth (Fig. 1b). The taper width and first grating length were checked every iteration to ensure the oxide semicircle at the taper-grating interface met the minimum enclosed area constraint for the GF Fotonix™process. Optimal device geometry was achieved in 142 iterations (Fig. 2c-e) (approximately 4 hours on a desktop computer).

Importantly, the area of the enclosed semicircle for the optimal geometry was consistently at the minimum enclosed area limit, suggesting that smaller feature sizes would enable increased reflection and that this is a peak reflectance limiting design constraint. This can be seen in Fig. 2c as the optimal taper width reduces to the smallest value allowed without resulting in a DRC violation. Smaller feature sizes allow more precise manipulation of the mode entering the gratings resulting in lower loss.

To accurately validate the performance of this device compared to the final device, the PO device was simulated in the time-domain Maxwell solver, MEEP [13]. The initial device design achieves a peak reflectance of 97.8 % at 1559 nm with a minimum reflectance of 97.2% over C-band (Fig. 2b). From this design, we employ topology optimization to further improve performance.

### *B. Topology Optimization*

Our TO algorithm is based on a hybrid time-frequency domain methodology [7] where we simulate the time-domain fields using MEEP [14] and accumulate the fields in a discrete-time Fourier transform. Using the adjoint variable method, we calculate the gradient of our device parameters (voxels of the design region) with respect to a user-specified objective function and evolve the topology of the device toward a locally optimal structure.

Our in-house TO pipeline enables simultaneous optimization of performance and satisfaction of factory DRC constraints [15]. However, this can cause conflicts in key areas where the two components of the optimization algorithm (performance and DRC compliance) compete, preventing the optimization algorithm from exploring additional perturbations [6]. The device designer can mitigate this effect by tuning hyperparameters which can be computationally expensive and ineffective. To circumvent this, we implement a mechanism that moves the design out of the local minimum caused by competing optimizations. This functionality enables the optimizer to find a superior local minimum that conforms to DRC.

We modify our existing TO pipeline by initializing the design region for the first iteration of TO with a filtered functional geometry. We then cycle through optimization via design region filtering and 12 iterations of traditional TO until reflectance is maximized (Fig. 3b). In the filtering stage, the design region is binarized and a blurring filter is used to add noise to the geometry, ensuring the optimizer perturbs the edges of the device. After the blurring filter, any minimum enclosed area violations are subtracted from the design region while any minimum area violations are added to the design region. This strictly enforces DRC while allowing the optimizer to make small modifications to the device geometry. Like in the PO case, the FOM, given in (5), was chosen to maximize reflectance.

The primary geometry of the gratings remains mostly unchanged by the optimization while the taper is optimized at the grating interface (Fig. 4c). This improves the transition between the waveguide and grating while remaining DRC compliant. This design process required less hyperparameter tuning compared to pure TO, resulting in far fewer total simulations. Seeding the optimization with a functional design also allowed us to reach an optimal design in 60 iterations (12 hours on a desktop computer) compared to over 200 iterations (40+ hours) for some pure TO designs [7].

The peak reflectance is improved by 1.1 % and shifted to 1569 nm while the C-band minimum reflectance is increased to 97.9 %. The reflectance remains over 98.3 % throughout L band, indicating strong broadband performance.

## IV. Device Analysis

In addition to the dual optimized HCG, a HCG of the same size was designed purely using TO. The topology of this structure is like the final HCG designed with dual optimizations but suffers in performance over C-band (Fig. 4a). The primary distinction between the two structures is in the waveguide taper and outer-grating region. The pure TO HCG lacks a taper which results in additional coupling loss at the

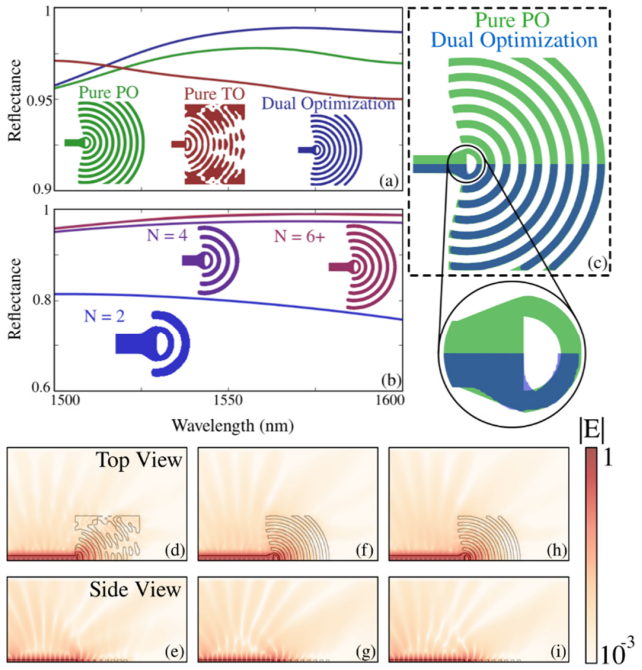


Fig. 4. (a) Simulated reflection spectra for the 3 HCG versions (dual optimization, PO, and pure TO). (b) Wavelength spectrum for dual optimized HCG with gratings removed. N denotes the number of grating periods. (c) Geometry of dual optimized HCG overlayed on the pure PO HCG. Top and side view of the normalized log-scale electric field magnitude for the pure TO (d-e), pure PO (f-g), and dual optimized (h-i) HCGs.

waveguide-grating interface. Like the PO HCG, the pure TO HCG includes apodization in the pitch of the gratings close to the waveguide that enhances reflected power. Contrary to the PO and dual optimized devices, the pure TO device does not conform to DRC due to small features on the edges of the device. Our TO algorithm cannot explore the entire design space due to the massive number of degrees of freedom and instead iteratively optimizes a grey design region towards a functional binary design. Conversely, the PO design is informed by the physics of similar devices, resulting in fewer degrees of freedom that can be more effectively explored.

The simulated continuous wave fields (Fig. 4d-i) reveal the direction of lost power. The scattered light is remarkably similar for the PO and dual optimized devices. Much of the lost power is scattered out of plane into the space above and below the grating. Moreover, to analyze the effectiveness of the HCG structure, gratings were systematically removed, and the reflectance of each modified design was simulated (Fig. 4b). The reduced device with 6 grating periods (N = 6) achieves the same spectrum as the optimal device with a shorter length (3 $\mu$m). This indicates that no more than 6 gratings are necessary for a grating with this effective index contrast ($\Delta n \approx 1$) as minimal field reaches the outer gratings. This analysis enables the possibility of recasting the modified TO stage to yield a HCG in a smaller footprint with similar performance.

## V. Conclusion

A dual optimization approach utilizing both PO and TO is employed to intelligently optimize the geometry of an ultra-compact circular HCG. This design methodology reduces the computational complexity of the optimization problem compared to pure TO while achieving superior performance. The total time consumption for this optimization is approximately 16 hours. The optimized device has a minimum reflectance of 97.9 % over C-band in a compact footprint. The waveguide-grating interface geometry is critical to achieving maximum performance and the features of the interface indicate the performance is fabrication limited. This design methodology reveals features that are critical to achieving high performance but are not present in a pure TO design. It is likely that advancements to our pure TO pipeline can be made to ensure these features are properly explored by TO and may enable TO alone to achieve similar performance to our hybrid approach. However, this work demonstrates the usefulness of a hybrid approach to ensure user established design constraints allow TO to explore more of the design space and achieve a superior device geometry. This work also demonstrates that seeding TO with a known topology enables the design of ultra-compact, high performance, foundry compatible integrated photonic devices.

## Acknowledgment

The authors would like to thank GlobalFoundries for providing silicon fabrication through Fotonix™ university program.

## References

[1] X. Wang, S. Grist, J. Flueckiger, N. A. F. Jaeger, and L. Chrostowski, "Silicon photonic slot waveguide Bragg gratings and resonators," *Opt. Exp.*, vol. 21, no. 16, p. 19029, Aug. 2013.

[2] M. Burla, L. R. Cortés, M. Li, X. Wang, L. Chrostowski, and J. Azaña, "Integrated waveguide Bragg gratings for microwave photonics signal processing," *Opt. Exp.*, vol. 21, no. 21, p. 25120, Oct. 2013.

[3] G. Saha et al., "Parameter optimization of foundry-enabled modified Bragg grating filters," in *Proc. Integr. Photon. Res., Silicon Nanophotonics*, Jul. 2022, Paper JW3A-41.

[4] C. Xiang et al., "Ultra-narrow linewidth laser based on a semiconductor gain chip and extended SiN Bragg grating," *Opt. Lett.*, vol. 44, no. 15, pp. 3825–3828, Aug. 2019.

[5] S. Gao, Y. Wang, K. Wang, and E. Skafidas, "High contrast circular grating reflector on silicon-on-insulator platform," *Opt. Lett.*, vol. 41, no. 3, p. 520, Feb. 2016.

[6] R. P. Pesch, A. Khurana, J. B. Slaby, J. Hiesener, and S. E. Ralph, "Analysis of local optimization behavior: Toward a novel inverse design paradigm," in *Proc. IEEE Photon. Conf. (IPC)*, Nov. 2023, pp. 1–2.

[7] A. M. Hammond, "High-performance hybrid time/freq-domain topology optimization for large scale photonics inverse design," *Opt. Exp.*, vol. 30, no. 3, pp. 4467–4491, Jan. 2022.

[8] D. C. Flanders, H. Kogelnik, R. V. Schmidt, and C. V. Shank, "Grating filters for thin-film optical waveguides," *Appl. Phys. Lett.*, vol. 24, no. 4, pp. 194–196, Feb. 1974.

[9] L. Chrostowski, *Silicon Photonics Design: From Devices to Systems*. Cambridge, U.K.: Cambridge Univ. Press, Mar. 2015.

[10] A. Li, "Ultra compact Bragg grating devices with broadband selectivity," *Opt. Lett.*, vol. 45, no. 3, pp. 644–647, Feb. 2020.

[11] *Lumerical Solutions*, Inc. Accessed: Dec. 11, 2023. [Online]. Available: http://www.lumerical.com/tcad products/fdtd/

[12] *The MathWorks, Inc.* Accessed: Dec. 11, 2023. [Online]. Available: https://www.mathworks.com/help/stats/bayesopt.html

[13] A. D. Bull, "Convergence rates of efficient global optimization algorithms," *J. Mach. Learn. Res.*, vol. 12, no. 10, pp. 1–26, Oct. 2011.

[14] A. F. Oskooi, D. Roundy, M. Ibanescu, P. Bermel, J. D. Joannopoulos, and S. G. Johnson, "MEEP: A flexible free-software package for electromagnetic simulations by the FDTD method," *Comput. Phys. Commun.*, vol. 181, no. 3, pp. 687–702, Mar. 2010.

[15] A. M. Hammond, A. Oskooi, S. G. Johnson, and S. E. Ralph, "Photonic topology optimization with semiconductor-foundry design-rule constraints," *Opt. Exp.*, vol. 29, no. 15, p. 23916, Jul. 2021.